PERGAMON

Atmospheric Environment 35 (2001) 561–568

ATMOSPHERIC ENVIRONMENT

www.elsevier.com/locate/atmosenv

Raman spectroscopic characterization of carbonaceous aerosols

S.-K. Sze[a], N. Siddique[a], J.J. Sloan[a,*], R. Escribano[b]

[a]*Department of Chemistry, University of Waterloo, Waterloo, Ont., Canada N2L 3G1*
[b]*Consejo Superior de Investigaciones Cientificas, Instituto de Estructura de la Materia, Serrano, 123-28006, Madrid, Spain*

Received 24 March 2000; accepted 7 June 2000

Abstract

We have used Raman spectroscopy to characterize a variety of carbon-containing particulate matter, including samples collected in ambient urban atmospheres. Based on the Raman spectra of known, commercial particles, we derive a simple empirical model that reflects their microchemistry and microphysics. This model gives information on the crystal size and morphology of the graphitic component, which correlates with the known characteristics of the commercial samples. We derive similar information about the graphitic component of the ambient particles, and suggest that this method might be used to characterize ambient particles systematically in the future.

Keywords: Particulate matter; Carbon; Graphite; Urban atmosphere; Pollution

1. Introduction

There is a growing body of clinical evidence indicating that adverse public health effects are caused by the presence of respirable or inhalable particulate matter (PM) in the ambient air (Neukirch et al., 1998). Particles with diameters smaller than 10 μm (denoted PM_{10}) are problematic. The deleterious effects increase with decreasing size. The most significant dangers occur for particles smaller than 2.5 μm ($PM_{2.5}$) (Monn et al., 1997; Wilson and Suh, 1997) because these penetrate deeply into the lungs, from where they cannot be removed by respiration.

Of course, particles are not dangerous simply because they are small, but rather because of the material on and in them, which they carry into the lungs. In urban atmospheres, the chemical makeup of this material is quite complex (Kleeman and Cass, 1998) but carbon compounds (both elemental and organic) usually comprise the largest fraction of these particles. This is especially true of particles produced by motor vehicles (Kirchstetter et al., 1999) but is equally true of many other important classes of particles, including secondary organic aerosols (Barthelmie and Pryor, 1997) as well as those produced in cooking and many common industrial processes.

There is a great deal of evidence supporting the correlation between high PM levels and effects on public health (Siegmann et al., 1999), much of which deals with the detrimental effects of carbon-based particles specifically (Hoek et al., 1997). Diesel soot is thought to be especially dangerous because it is a possible carcinogen (International agency for research on cancer, 1989). For this material, the US Environmental Protection Agency (1993) has proposed an inhalation reference concentration of only $5\,\mu g\,m^{-3}$.

Because of these public health dangers, it is important to have accurate and sensitive analytical methods for the detection and analysis of carbonaceous particles. Chemical speciation of these particles, however, is difficult due to their complexity. The routine analyses that support air quality standards in many jurisdictions require only the determination of the mass (as opposed to the chemical composition) of the PM_{10} fraction. Although the need for more complete chemical information is clear, the

* Corresponding author. Fax: +1-519-746-0435.
E-mail address: sloanj@uwaterloo.ca (J.J. Sloan).

1352-2310/00/$ - see front matter
PII: S1352-2310(00)00325-3

methods presently available for chemical speciation of urban particles require extensive laboratory work and are not implemented for routine air quality monitoring in any jurisdiction of which we are aware.

Optical spectroscopy is an especially powerful tool for chemical analysis, which has been used for many years to get chemical information about bulk phases. Infrared (IR) and Raman measurements have especially high selectivity, giving information not only about the identity of molecules and crystals, but about their immediate environment as well. The mid-IR "fingerprint" region gives excellent selectivity for chemical speciation and although its application to micron-sized particles is somewhat complicated by the effects of light scattering, when combined with appropriate spectral computations, it is capable of determining the chemical composition, phase and size distribution of most aerosol samples. We have used IR spectroscopy and optical computations extensively to determine the atmospheric extinction spectra of stratospheric clouds and aerosols for interpretation of satellite, aircraft and balloon measurements (see, for example, Bertram and Sloan, 1998 and references therein).

While direct IR extinction measurements on aerosols can provide a wealth of information, their sensitivity is not particularly high, and a substantial effort can be involved in extracting unambiguous information about the particles. By comparison with IR measurements, Raman spectroscopy of particles can provide higher sensitivity with comparable selectivity. While it provides little information about particle size, Raman spectroscopy more than compensates for this with its capability for chemical speciation. Carbon compounds have particularly large transition strengths for Raman scattering, which has been used very widely in materials science to monitor the properties of carbon nanotubes, synthetic diamonds, etc. Despite these advantages, however, it has not been used much for measurements of ambient particles. Despite some early suggestions that it might be useful in this application (Blaha et al., 1978; Rosen and Novakov, 1978) its use has been limited to well-controlled laboratory conditions (Lubben and Schrader, 1997) and synthetic aerosols (Ayora et al., 1997). Recently, a very informative discussion of the theory of Raman spectroscopy of aerosols has appeared (Schweiger, 1999).

We have undertaken to explore the use of Raman spectroscopy for the characterization of urban carbonaceous particles, for the reasons outlined above. We have constructed a laboratory Raman apparatus for this purpose, rather than purchasing a commercial instrument, because of the extra flexibility this approach affords. During the development of this apparatus, we monitored its capabilities by reproducing measurements of various commercial carbon and graphite particles that had been reported previously in the literature. After the construction and development of the apparatus, we used it to measure the Raman spectra of ambient urban particles collected by our collaborators in the Monitoring and Reporting Branch of the Ontario Ministry of the Environment. We summarize these initial experiments in the following report and assess their results.

2. Experimental apparatus

Most conventional methods for sampling ambient particles involve their collection on filters. Because it is desirable to avoid excessive manipulation of the samples, we designed the Raman apparatus to record the spectra of particles directly from the filters used to collect them. This approach gives acceptable results for common filters composed of pure quartz fibres or metal membranes. Filter materials made with inorganic binders, and filters made from Teflon, polycarbonate or other polymeric materials, however, give unacceptable levels of background fluorescence and cannot be used.

The configuration of the Raman spectrometer is conventional in most respects. The excitation source is a Coherent Inc. argon ion laser operating in multiline mode. A 60° prism is used to disperse the laser light and the 514.5 nm line is isolated using an aperture. The laser beam is focused to a spot of about 100 μm diameter at the sample using a 20 cm focal length lens; it is incident on the sample at a grazing angle to the plane of the filter. Depending on the sample, laser powers in the range from 10 to 300 mW provided adequate signal to noise. The lower end of this range was used in most cases to avoid excessive sample heating. In the event that higher powers need to be used, however, we found that sample damage could be minimized by the use of metal substrates such as silver membrane filters (Osmonics Inc.) which have high thermal conductivity. These are considerably more expensive than quartz filters, so we did not use them extensively.

The Raman signal is collected by an $f/1.2$ lens having its axis perpendicular to the filter and located at its focal distance from the sample. The collected light is passed through a holographic notch filter (Kaiser Optical Systems Inc.) to remove the Rayleigh scattering. An $f/4.7$ lens focuses the signal into the entrance slit of a single-pass McPherson monochromator (model 207, $f/4.7$, 0.67 m) with a slit width of 200 μm. This yields a resolution of about $10\,cm^{-1}$. A photomultiplier tube (Hamamatsu R3896, cooled to −100°C) detects the signal. Its output is fed to a lock-in-amplifier referenced to a 3400 Hz optical chopper used to modulate the laser beam. The monochromator is scanned over the range from about 516 to 630 nm.

This apparatus was used to measure the Raman spectra of several carbonaceous particle samples. For purposes of calibration, we recorded the spectra of various commercially obtained carbon and graphite samples.

Following this, we recorded the spectra of several samples that had been collected from ambient urban air in Hamilton, Ontario by the Monitoring and Reporting Branch of the Ontario Ministry of the Environment. The information gained from the spectra of the known commercial samples provided significant insight into the spectra of the ambient PM.

3. Results

We show the Raman spectra of six different samples of commercially obtained graphite and carbon particles in Fig. 1. All of these were obtained from Alfa Aesar Inc., except Number 28286-3, which came from Aldrich Chemical Co and FW2, from Degussa Corporation. The properties of these particles, provided by the suppliers, are listed in Table 1.

The Raman spectra of the various forms of graphite have been discussed extensively in the literature, beginning more that 30 yr ago (Nathan et al., 1974; Tuinstra and Koenig, 1970). The first-order transitions lie between 1200 and 1700 cm^{-1}, while the second-order transitions are near 2700 cm^{-1}, extending to about 3500 cm^{-1}. The shapes and intensities of the Raman transitions are functions of the graphite crystal size, morphology and sample composition. Even without detailed analyses of the spectra in Fig. 1, their comparison with the corresponding information in Table 1 suggests that qualitative information about the microstructure of the samples may be derived from the strengths and widths of the spectral features in a relatively simple way.

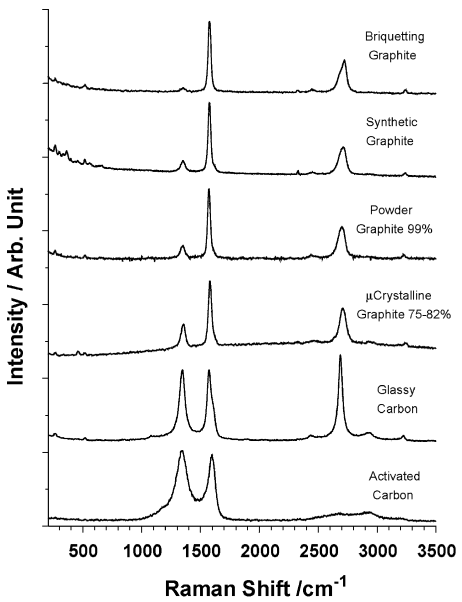

Fig. 1. The Raman spectra of a series of commercial samples containing various amounts of crystalline graphite.

The particles are composed of both crystalline graphite and a non-graphite component, which in most cases is an unknown mixture of sp^2- and sp^3-bonded carbon with no long-range order. For convenience, we will refer to this as amorphous carbon. Roughly speaking, both the crystal size and graphite content of the samples decrease from top to bottom in Fig. 1. Examination of the region between 1200 and 1800 cm^{-1}, shown in Fig. 2, illustrates this. We have inserted vertical reference lines at 1360, 1585 and 1620 cm^{-1} to indicate the presence of the three most important features in this region of the spectrum. All have been discussed extensively in the literature (Dresselhaus and Dresselhaus, 1982; Wang et al., 1990). The feature at 1585 cm^{-1}, denoted the G peak, is the E_{2g} mode of bulk crystalline graphite. This is the fundamental mode of the graphite crystal; its intensity scales with the crystal size. Dresselhaus and Dresselhaus (1982) assign the 1620 cm^{-1} feature to the analogue of the E_{2g} mode for the graphite layers located at the boundary of the crystals, and suggest the designation E'_{2g} (D′). The 1620 cm^{-1} feature is sensitive to the composition of the material in contact with the surface layers of the graphite, which modifies their electronic environment. The upward shift is caused either by the altered electronic environment of this "boundary" plane or by its reduced symmetry.

The feature near 1360 cm^{-1}, designated the D (disorder) band, is allowed only if the $k = 0$ selection rule breaks down, which occurs near crystal edges. Wang et al. (1990) have suggested that this band originates in the edge vibrations since its frequency is independent of chemical composition or sample preparation. Also, Compagnini et al. (1997) provide further evidence for the correlation of this feature with the graphite edge planes. Its frequency depends somewhat on the frequency of the excitation laser, and attempts to explain this property also help to illuminate the spectroscopic origins of this band (Pocsik et al., 1998). Recently, Matthews et al. (1999) have refined this suggestion by proposing that the D band is a π–π^* transition near the K point in the (2D) graphite reciprocal lattice, enhanced by strong coupling between the optic and the transverse acoustic phonon branches at this point. This explains why the frequency of this band is strongly dependent on the wavelength of the excitation laser, and empirical correlations such as the ones we will suggest later in this paper must account for this point.

In view of their assignments, it seems clear that the relative intensities of these features can be used to give information about the sizes and morphologies of the graphite crystals. The G peak indicates the presence of large graphite crystals, while the ratio of the D to G peaks gives the relative amount of edge to volume of the crystals. The frequency of the D′ peak gives information about the electronic environment near the surface layers of the particles while its intensity relative to that of

Table 1

Number	Name	Description
14735	Briquetting grade graphite	Mined graphite, 99.9995% (metals basis). Sieved (100 mesh) purified at $>2000^{\circ}C$ under low pressure
28286-3	Synthetic graphite (purified)	99.9%, 1–2 μm particles, air-milled, purified at $3000^{\circ}C$
10129	Synthetic graphite	99%, 300 mesh powder, from desulphurized petroleum coke
10130	Graphite powder, microcrystalline	Mined graphite 75–82% C, 18–25% ash, milled (300 mesh) unpurified
38008	Glassy carbon spherical powder type 2	Synthetic, from phenolic resin, 0.4–12 μm
FW2	Carbon black	Printer Ink, 13 μm particle size
33302	Activated carbon	Powder; ash 4% maximum

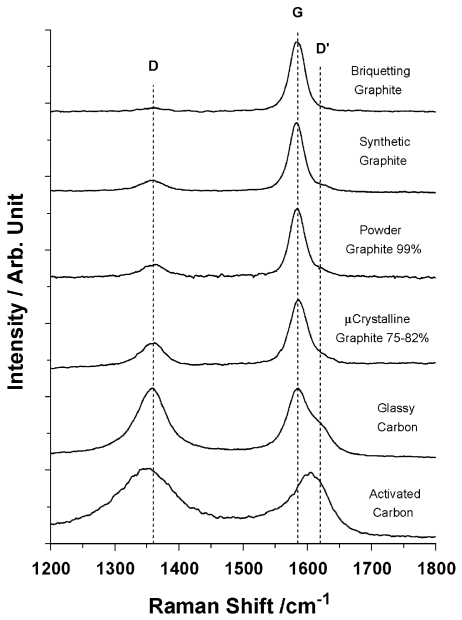

Fig. 2. Raman spectra of carbon samples in the first-order region, showing the locations of the three major transitions discussed in this paper.

the G peak gives a measure of the surface to volume ratio of the particles. We are presently developing a model, using these simple ideas, to derive the morphology and composition of carbonaceous particles, based on the appearance of their Raman spectra. We hope to use this model to characterize particles formed in different combustion processes. Since different kinds of carbonaceous particles are formed in diesel and spark ignition engines, the burning of coal and other fossil fuels for power generation and other kinds of combustion such as biomass burning, we suggest that the features of the Raman spectra of the particles might be used to identify the sources of such particles. As examples of this, we will show the Raman spectra of several ambient particles collected in various urban locations and compare their characteristics according to the above criteria.

3.1. Diesel particles

Using silver membrane filters, we collected PM from the exhaust of a diesel tractor (John Deer, Model No. E444) at the University of Waterloo. Fig. 3 shows the spectra of particles collected on filters having pore sizes of 0.8 μm (top) and 5.0 μm (middle). The bottom trace in Fig. 3 shows the spectrum of a sample of particles collected near a heavy traffic area of Madrid, Spain. The similarity with the other spectra is striking, indicating that most of the latter were likely produced by diesel vehicles. The spectrum of the diesel tractor PM collected on the filter having the smaller pore size, shows a strong peak at a Raman shift of $975\,cm^{-1}$ corresponding to $(NH_4)_2SO_4$ and a smaller peak corresponding to NH_4NO_3 at $1055\,cm^{-1}$. We do not know the origin of these materials, but since the major use of the tractor was in landscaping, we assume they originate, at least in part, from ammonium fertilizer.

Vertical dashed lines indicate the D, G and D′ peaks. For all of these particles, the maximum of the D line is at $1395\,cm^{-1}$, displaced by about $35\,cm^{-1}$ to higher frequency as compared to its location in the glassy and activated carbon samples shown in Fig. 2. Also, in all cases, the strongest feature is the D′ line, and there is no obvious evidence of the G line. These relative intensities suggest that the surface to volume ratio of the graphite crystals is large. Moreover, the large shift in the maximum of the D line suggests that the edges might be chemically modified by the diesel combustion in a way that changes the electronic environment for the edge vibrations.

3.2. Urban particles

We have also recorded the spectra of several samples of PM collected in Hamilton, Ontario, by the Ontario Ministry of the Environment. These samples were

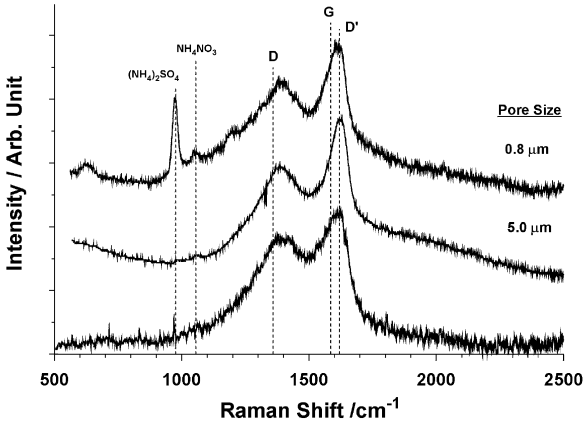

Fig. 3. Raman spectra of three soot samples collected from a diesel tractor (top two curves) and a street in Madrid, Spain (bottom curve). The shifts in the locations of the three indicated graphite transitions, as compared with their locations in Fig. 2 indicate morphological or microphysical differences.

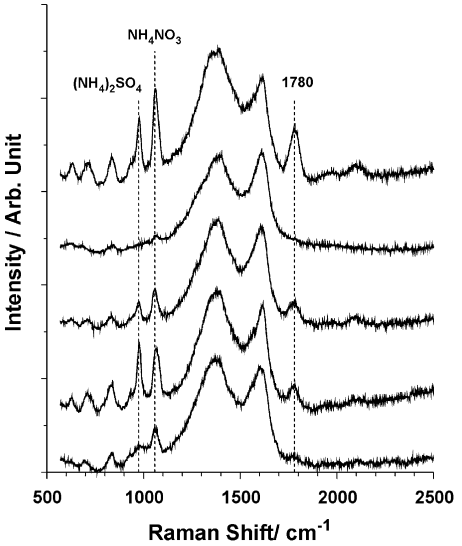

Fig. 4. Raman spectra of five different soot samples collected on quartz (Hi-Vol) filters at various times from a street location in Hamilton, Ontario. The episodic occurrence of inorganic material is evident, as are the small differences among the graphite signatures in the various samples.

collected on quartz filters using Hi-Vol samplers in the course of routine PM monitoring activities. Hamilton is an industrial area having refineries, smelters and a wide variety of vehicles having both diesel and spark ignition engines. These samples are the PM_{10} fraction from the sampler, so they represent all sizes below 10 μm diameter.

The samples contain a wide variety of PM, and the spectra are complex. In some cases, broadband fluorescence was observed from these samples. And for cases where the particle number density was small, this affected the baseline significantly. In those cases for which we wanted to measure the line areas of such samples, we removed the fluorescence signal by subtracting a fourth-order polynomial that had been fitted to the baseline. Even in these cases, however, the carbon peaks predominate over the spectral noise. Fig. 4 shows five examples of these spectra. In addition to the D, G and D′ peaks, some of the samples show $(NH_4)_2SO_4$ and NH_4NO_3 peaks, as well as several other unidentified bands, including one at about 1780 cm^{-1}, indicated by a vertical dashed line, that is close to the characteristic Raman frequency of the carbonyl group. In contrast to the diesel particles, the frequencies of the three graphite peaks in these spectra are much closer to those in the corresponding spectra of pure graphite samples. We attribute this to the different origins of the particles and in particular to the fact that the Hamilton samples likely contain a much lower fraction of diesel particles than those shown in Fig. 3.

3.3. Characterization of graphitic component

In order to use the characteristics of the particles to determine their origins, it is necessary to quantify the graphitic component. The D, G and D′ features give information about the size and shape of the graphite crystals, so they are the obvious choices for this purpose. The spectroscopic origins of these transitions are understood, and it is possible to derive considerable information about the microscopic characteristics of the sample on a theoretical basis. We will discuss this theory in a separate publication, report its application to problems like this and summarize the information that can be derived from it. For the present purposes, however, we use an empirical approach, in which we show that the relative areas of the three features depend on the origins of the particles, as described in Table 1. To get the areas of the features, we use a commercial fitting program, *Grams 32* (Galactic Industries Ltd.). For the fitting procedure, we specify Lorentzian lineshapes at the frequencies of the D, G and D′ transitions, and allow these to vary slightly, within the resolution of the spectrometer. Then the program adjusts the amplitudes of the lines to get the best overall fit to the measured spectrum and reports the integrated areas for the three lines. We also carried out the fits using Gaussian lineshapes and found that in all cases the graphitic features were better fitted by Lorentzians. This, of course, is consistent with the line broadening mechanism expected for these samples.

We carried out this procedure for each of the samples shown in Figs. 1 and 2, as well as a large number of those collected from the ambient atmosphere. We show examples of the resulting fits in Figs. 5 and 6. Here we focus

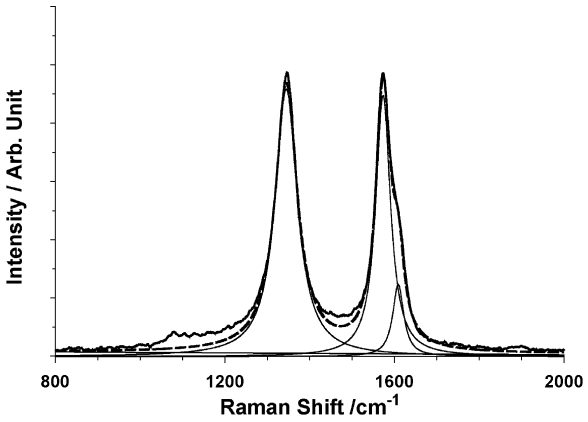

Fig. 5. Raman spectrum of glassy carbon particulates fitted using three Lorentzian curves located at the frequencies of the D, G and D′ bands. Thin solid curves (3): Lorentzians. Heavy solid curve (noisy): measured spectrum. Dashed curve: sum of Lorentzians.

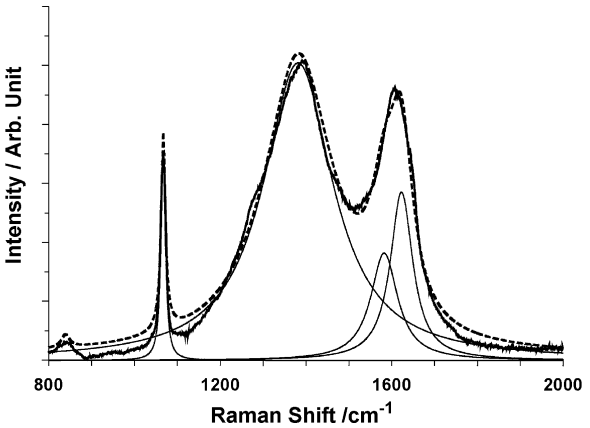

Fig. 6. Raman spectrum of urban particulates from same location as those of Fig. 3, fitted using four Lorentzian curves – one at the NH_4NO_3 band and the others as in Fig. 4.

only on the first-order spectrum to emphasize the details of the fit. In both cases, the measured spectrum and individual fitted peaks are solid curves; the total fitted spectrum, which is the sum of the latter, is a dashed curve. Fig. 5 shows the result for the glassy carbon spectrum shown in Fig. 1. Fig. 6 shows the fit of the three graphitic peaks detected on a quartz fibre Hi-Vol filter collected by the Measuring and Reporting Branch of the Ontario Ministry of the Environment.

For the glassy carbon sample in Fig. 5, we do not recover the entire signal in the wings of the D peak, whereas we do so very well for the G and D′ peaks. The signal not retrieved by the fit originates in a secondary maximum about $250\,cm^{-1}$ below the main transition. This feature is also evident in the second-order spectrum of glassy carbon shown in Fig. 1. For our present purposes, we are concerned only with the major transitions, so we will ignore this discrepancy. We will discuss this and other detailed spectroscopic information in a forthcoming paper. The D′ peak in this case is much smaller than the G peak and is shifted to higher frequency by about $36\,cm^{-1}$. This shift is consistent with that expected from the known graphite spectroscopy (Dresselhaus and Dresselhaus, 1982). For the ambient particles shown in Fig. 6, the fit of the three graphite bands is not as good as that for the purer sample in Fig. 5, but the spectrum nevertheless is recovered satisfactorily by the fitted curve (dashed). In this case, there is a strong peak due to ammonium nitrate at $1055\,cm^{-1}$, as well as a smaller one near $850\,cm^{-1}$, which we are unable to identify. Both were included in the simulation, to get the best accuracy for all fitted peaks. For the ambient sample, the D′ peak is also shifted to higher frequency than the G peak by about $40\,cm^{-1}$ but unlike the higher purity samples (the first five in Table 1) it is much more intense than the former. This is a characteristic of all the ambient samples we have measured. We will discuss the implications of this in the next section.

4. Discussion

Differences in the relative sizes and shapes of the three Raman peaks that are the focus of this report contain information about the morphology of the graphite crystals. This is because the modes responsible for them are influenced by the microphysical states of the crystals and their detailed chemical compositions. The morphology, in turn, is related to the process in which the graphitic sample is produced (see Table 1). Thus the Raman spectrum of the sample should give some indication of the particle's origin. To make this correlation, we assume that the intensities of the respective transitions reflect the amount of the crystal that participates in the corresponding vibrational mode. This measurement is expressed quantitatively through the Raman polarizability, but for the present purposes, we shall restrict ourselves to an empirical comparison of the intensities. In a later publication, we will discuss the computations of the absolute intensities.

The three carbon bands recorded in this work all originate from crystalline graphite. The differences among the spectra arise from two main sources: differences in the crystal size and morphology and differences in the composition of the material in which the crystals are embedded. The former cause larger effects than the latter. Additional information can be derived from the small frequency shifts caused by second-order effects; those will be considered in a later paper. Although the morphologies of the graphite crystals are very

complicated, to simplify the discussion we will interpret the results in terms of rhomboidal crystal geometry. This includes pillars or rods having any cross-sectional shape and arbitrary length to height ratios. The essential concepts to be discussed are not changed by the particular shapes, but the values of the parameters obtained do depend on the geometry. The general discussion, however, requires only that the top and bottom surfaces be distinguishable from the remaining (edge) surfaces, and that the Raman-active surface modes be different from those of the bulk. For purposes of illustration, we will frame the following discussion in terms of the simplest geometrical example – a cylinder.

The G transition is the E_{2g} mode of bulk crystalline graphite. Thus we take its intensity to be a measure of the average volume of the ordered graphite crystals in the sample. The intensity of the D band is known to be inversely proportional to the average crystal size (within a certain range). It is only observed for crystals smaller than a few tens of nanometers, and its precise origin is still somewhat in doubt. There is a thorough discussion of this band in Wang et al. (1990), which concludes that it becomes allowed as a result of symmetry breaking at the edges of the graphite crystals. In keeping with this, we will take the D band intensity to be a measure of the total area of the crystal edges. In the cylindrical approximation, therefore, the ratio of the D band intensity to that of the G band would be inversely proportional to the radius of the crystal. The D′ transition originates in surface modes, and thus is characteristic of layers which have a graphite layer on one side and something else on the other. While its Raman polarizability is influenced to some extent by the identity of the material in contact with the surface, we will ignore this effect for the present. We assume, therefore, that the D′ intensity reflects the surface area of the average crystal, without consideration of its local surroundings. In the cylindrical approximation, the ratio of the D′ peak to the G peak is inversely proportional to the average thickness of the crystals.

These suggestions can be tested using X-ray diffraction measurements of graphite crystals having known sizes and morphologies. Studies of this kind have been reported in the literature for some time (McCulloch et al., 1994; Tuinstra and Koenig, 1970) especially in the context of carbon nanotubes (Richter and Subbaswamy, 1997), and in most cases they confirm the general validity of these empirical approximations. The relative intensities, however, depend on many other influences such as the wavelength of the Raman laser, so it is not possible to derive quantitative information from these simple correlations. Nevertheless, it is instructive to examine the predictions of this simple model and compare them with the limited information available about the samples we have reported here.

In Fig. 7, we show the relative areas of the three graphite peaks, obtained using the fitting procedure

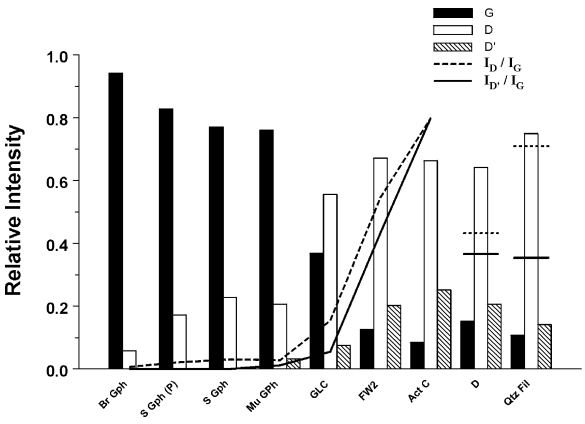

Fig. 7. Relative intensities of the D, G and D′ bands from various samples obtained from the areas of the Lorentzian curves fitted as in Figs. 5 and 6.

outlined in the previous section. The G, D and D′ areas are represented by the heights of the bars, from left to right in each group of three. The first seven groups of bars (left to right in the figure) correspond to the seven commercial samples listed in Table 1 (top to bottom). Of these, the first four contain mostly large graphite crystals, the next (Glassy Carbon) is composed of graphite "ribbons", and the last two consist mostly of amorphous carbon with some very small graphite crystals embedded in it. We have arranged these in the order of decreasing crystal size or purity of the graphite samples, as indicated by the information given to us by the suppliers. Clearly, this order also corresponds to decreasing intensity of the G peak and increasing intensities of the D and D′ peaks. In the first three samples, the D′ peak intensity is below our detection limit. The dashed and solid lines show the D/G and D′/G intensity ratios, respectively.

The last two groups of bars represent the data for the diesel soot sample shown in the middle spectrum of Fig. 3 (5.0 μm pore size) and the particles collected from urban air using a quartz filter (see Fig. 6). For these samples, the D/G ratio is much larger for the urban particles than for the diesel soot, whereas the D′/G ratios are similar. According to the simple model described above, this indicates that the apparent edge to volume ratio of the graphite particles on the quartz filter is significantly larger than that of the diesel soot, but that the apparent surface (planar) graphite to volume ratios are similar. Since these particles might have complex shapes, we cannot interpret these results in simple geometrical terms at the present time. It is clear, however, that the Raman spectra indicate that the crystals have significantly different morphologies. Next, it is necessary to examine systematically the correlations between these spectral features and the origins of the particles in which they are observed. In this way, it might be possible to

show that the characteristic morphologies of the particles that we have discussed here can be used to identify their sources.

Acknowledgements

This work was supported by funding from the Centre for Research in Earth and Space Technology (JJS), NATO (JJS and RE), and the Commonwealth Scholarship Program (NS). We are grateful to the Ontario Ministry of the Environment for provision of ambient PM samples and also acknowledge helpful discussions with Dr. Raymond Hoff.

References

Ayora, M.J., Baillestros, L., Persz, R., Latimer, H.K., et al., 1997. Detection of atmospheric contaminants in aerosols by surface-enhanced Raman spectrometry. Analytica Chimica Acta 355, 15–21.

Barthelmie, R.J., Pryor, S.C., 1997. Secondary organic aerosols: formation potential and ambient data. Science of the Total Environment 205, 167–178.

Bertram, A.K., Sloan, J.J., 1998. The nucleation rate constants and freezing mechanism of nitric acid trihydrate aerosol under stratospheric conditions. Journal of Geophysical Research D (Atmospheres) 103, 13261–13265.

Blaha, J.J., Rosasco, G.J., Etz, E.S., 1978. Raman microprobe characterization of residual carbonaceous material associated with urban airborne particulates. Applied Spectroscopy 32, 292–297.

Compagnini, G., Puglisi, O., Forti, G., 1997. Raman spectra of virgin and damaged graphite edge planes. Carbon 35, 1793–1797.

Dresselhaus, M.S., Dresselhaus, G., 1982. In: Cardona, M., Güntherodt, G. (Eds.), Light Scattering in Solids, Vol. III. Springer, Berlin, pp. 3–58.

Hoek, G., Schwartz, J.D., Groot, B., Eilers, P., 1997. Effects of ambient particulate matter and ozone on daily mortality in Rotterdam, The Netherlands. Archives of Environmental Health 52, 455–463.

International Agency for Research on Cancer, 1989. IARC Monographs on the Evaluation of Carcinogenic Risks to Humans of Diesel and Gasoline Exhausts and some Nitroarenes, Vol. 49. World Health Organization, Lyon, France.

Kirchstetter, T.W., Harley, R.A., Kreisberg, N.M., Stolzenburg, M.R., et al., 1999. On-road measurement of fine particle and nitrogen oxide emissions from light- and heavy-duty motor vehicles. Atmospheric Environment 33, 2955–2968.

Kleeman, M.J., Cass, G.R., 1998. Source contributions to the size and composition distribution of urban particulate air pollution. Atmospheric Environment 32, 2803–2816.

Lubben, J.F., Schrader, B., 1997. Chemical composition analysis and temperature determination of optically levitated single aerosol particles by means of a compact Raman spectrometer. Journal of Molecular Structure 410–411, 543–546.

Matthews, M.J., Pimenta, M.A., Dresselhaus, G., Dresselhaus, M.S., et al., 1999. Origin of dispersive effects of the Raman D band in carbon materials. Physical Review B 59, R6585–R6588.

McCulloch, D.G., Prawer, S., Hoffman, A., 1994. Structural investigation of xenon-ion-beam-irradiated glassy carbon. Physical Review B 50, 5905–5917.

Monn, C., Fuchs, A., Hogger, D., Junker, M.,, et al., 1997. Particulate matter less than 10 μm (PM10) and fine particles less than 2.5 μm (PM2.5): relationships between indoor, outdoor and personal concentrations. Science of the Total Environment 208, 15–21.

Nathan, M.I., Smith Jr., J.E., Tu, K.N., 1974. Raman spectrum of glassy carbon. Journal of Applied Physics 45, 2370–2371.

Neukirch, F., Segala, C., Le Moullec, Y., Korobaeff, M., et al., 1998. Short-term effects of low-level winter pollution on respiratory health of asthmatic adults. Archives of Environmental Health 53, 320–328.

Pocsik, I., Hundhausen, M., Koos, M., Ley, L., 1998. Origin of the D peak in the Raman spectrum of microcrystalline graphite. Journal of Non-Crystalline Solids 230, 1083–1086.

Richter, E., Subbaswamy, K.R., 1997. Theory of size-dependent resonance Raman scattering from carbon nanotubes. Physical Review Letters 79, 2738–2741.

Rosen, H., Novakov, T., 1978. Identification of primary particulate carbon and sulfate species by Raman spectroscopy. Atmospheric Environment 12, 923–927.

Schweiger, G., 1999. In: Spurney, K.R. (Ed.), Analytical Chemistry of Aerosols. Lewis Publishers, Boca Raton, FL, pp. 319–352.

Siegmann, K., Scherrer, L., Siegmann, H.C., 1999. Physical and chemical properties of airborne nanoscale particles and how to measure the impact on human health. Theochem-Journal of Molecular Structure 458, 191–201.

Tuinstra, F., Koenig, J.L., 1970. Raman spectrum of graphite. Journal of Chemical Physics 53, 1126–1130.

US Environmental Protection Agency, 1993. Health assessment document for diesel emission. EPA/600/8-90/057A, Office of Health and Environmental Assessment, Environmental Criteria Office, Research Triangle Park, NC.

Wang, Y., Alsmeyer, D.C., McCreery, R.L., 1990. Raman spectroscopy of carbon materials: structural basis of observed spectra. Chemistry of Materials 2, 557–563.

Wilson, W.E., Suh, H.H., 1997. Fine particles and coarse particles: concentration relationships relevant to epidemiologic studies. Journal of the Air and Waste Management Association 47, 1238–1249.